Revision 2

Wenlanzhangite–(Y) from the Yushui deposit, South China: a potential proxy for tracing the redox state of ore formation

Peng Liu[1*], Guowu Li[2], Ningyue Sun[2], Wei Yao[1,3], Hong Yu[4], Yongfei Tian[2], Wenqiang Yang[1], Fengshang Zhao[1], Nigel J. Cook[5]

[1] State Key Laboratory of Continental Dynamics, Department of Geology, Northwest University, Xi'an 710069, China

[2] Crystal Structure Laboratory, Science Research Institute, China University of Geosciences, 100083 Beijing, China

[3] Xi'an Center of Mineral Resources Survey, China Geological Survey, Xi'an 710100, China

[4] Ministry of Natural Resources (MNR) Key Laboratory of Metallogeny and Mineral Assessment, Institute of Mineral Resources, Chinese Academy of Geological Sciences (CAGS), Beijing 100037, China

[5] School of Chemical Engineering, The University of Adelaide, Adelaide, South Australia 5005, Australia

Corresponding author: Peng Liu, pengliu@nwu.edu.cn

This is the peer-reviewed, final accepted version for American Mineralogist, published by the Mineralogical Society of America.
The published version is subject to change. Cite as Authors (Year) Title. American Mineralogist, in press.
DOI: https://doi.org/10.2138/am-2023-9220. http://www.minsocam.org/

ABSTRACT

Mineral phases in which vanadium (V) and heavy–rare–earth elements (HREEs) coexist are rarely documented. Here, we report a new V–HREE–bearing silicate mineral species, wenlanzhangite–(Y), which is a vanadiferous derivate of jingwenite–(Y) [$Y_2Al_2V^{4+}{}_2(SiO_4)_2O_4(OH)_4$] coexisting with jingwenite–(Y) in bedded/massive ores at Yushui, South China. Wenlanzhangite–(Y) forms as a dark brown, 70–100 μm–thick rim on a core domain of jingwenite–(Y), which occurs as 100–200 μm columnar crystals. The colour, streak, lustre, and hardness (Mohs) are dark brown, yellow grey, vitreous, and ~4, respectively. Compared to jingwenite–(Y), wenlanzhangite–(Y) has higher vanadium and lower aluminium contents. Calculated on the basis of 8 cations, the empirical formula is $(Y_{1.26}Dy_{0.17}Er_{0.11}Gd_{0.09}Yb_{0.09}Nd_{0.09}Sm_{0.06}Sc_{0.04}Ho_{0.03}Ce_{0.02}Tb_{0.02}Tm_{0.02}Pr_{0.01})_{\Sigma 2.00}(V^{3+}{}_{1.46}Al_{0.54})_{\Sigma 2.00}V^{4+}{}_2(SiO_4)_2O_4(OH)_4$, which can be simplified to the ideal formula $Y_2V^{3+}{}_2V^{4+}{}_2(SiO_4)_2O_4(OH)_4$.

Wenlanzhangite–(Y) is triclinic, with space group P–1(#2), Z = 2, and unit–cell parameters a = 5.9632(7) Å, b = 9.599(1) Å, c = 9.9170(9) Å, α = 90.033(8)°, β = 98.595(2)°, γ = 90.003(9)°, and V = 561.28(10) Å^3. Wenlanzhangite–(Y) is approved by the International Mineralogical Association Commission on New Minerals, Nomenclature and Classification (IMA2022–142). The structure of wenlanzhangite–(Y) is composed of a–axis–oriented chains of [VO_6] octahedra consisting of edge–sharing octahedra linked by insular [SiO_4] tetrahedra, leaving open channels occupied by rare earth elements. Observed compositional variation and crystal structure demonstrate that V^{3+} can substitute for Al^{3+} in jingwenite–(Y), forming wenlanzhangite–(Y). The occurrence of wenlanzhangite–(Y) indicates a relatively more reducing hydrothermal environment causing reduction of V^{5+} in oxidized fluids to V^{3+} and thus represents a useful proxy for tracing the redox state of ore formation.

***Keywords*:** New mineral; Wenlanzhangite–(Y); Heavy rare earth elements; Yushui Cu deposit

INTRODUCTION

Recent studies have reported the first account of significant HREE (and associated U) mineralization within a sediment–hosted Cu deposit, the Yushui deposit, South China (Liu et al. 2023). It is well known that sandstone–hosted uranium deposits can host economic concentrations of V (e.g., Colorado Plateau, USA) (Dahlkamp 2010), and form at an oxidation–reduction interface (Northrop et al. 1990; Shawe 2011). Vanadium, as V^{3+}, V^{4+}, V^{5+}, or a combination thereof, can occur as oxide phases or is combined with redox–sensitive elements (Weeks et al. 1959). In practice, V–HREE–bearing mineral phases are rarely documented.

A new V–HREE–bearing silicate mineral, jingwenite–(Y) [$Y_2Al_2V^{4+}{}_2(SiO_4)_2O_4(OH)_4$], has been discovered and is an abundant phase in the Yushui deposit (Liu et al. 2023). Here we describe a vanadiferous derivate of jingwenite–(Y) from Yushui, wenlanzhangite–(Y), ideally $Y_2V^{3+}{}_2V^{4+}{}_2(SiO_4)_2O_4(OH)_4$. Wenlanzhangite–(Y) has been approved by the International Mineralogical Association Commission on New Minerals, Nomenclature and Classification (IMA2022–142). It is named in honor of Professor Wenlan Zhang (born in 1957), a famous expert in electron probe microbeam analysis at the School of Earth Sciences and Engineering, Nanjing University, China. She has published more than 80 papers that contribute to improvements and capabilities of electron probe analysis technology in China. Type material is deposited in the mineralogical collections of the Geological Museum of China, catalogue number GMCTM 2202.

GEOLOGICAL BACKGROUND

The Yushui deposit, located in the southwestern domain of the southeastern coastal belt, South China (Fig. 1a), is a small yet high–grade Cu deposit with significant HREE enrichment, and minor enrichment in U, Co, and V (Liu et al. 2023). Mineralization is concealed beneath Late–Jurassic volcanic cover and is hosted at the unconformity between Upper Carboniferous dark grey dolostone/limestone with organic– and apatite–rich beds and a >300 m–thick sequence of Lower Carboniferous red sandstone (Figs. 1, 2a, and 2b) characterized by an abundance of heavy minerals

including clastic xenotime–(Y), rutile, zircon, and hematite. There are three types of Cu ore: I) bedded/massive; II) disseminated; and III) vein–type (Fig. 2c–g). HREE–bearing minerals occur mainly in bedded/massive ore (orebody V_1). Based on mineral assemblages, orebody V_1 can be split into: I) a lower chalcopyrite–rich part; and II) an upper galena–rich part. The lower part is characterized by chalcopyrite, and abundant HREE–V– and V–Sc–bearing minerals including nolanite, thortveitite, roscoelite, xenotime–(Y), jingwenite–(Y) (Liu et al. 2023), hingganite–(Y), bastnäsite–(Y) and an unknown V–HREE–Sc–bearing silicate mineral phase. Minor components include bornite, barite, sphalerite, galena, uraninite, and quartz. The upper part of the orebody underlies the dolostone, and is dominated by galena, sphalerite, bornite, chalcopyrite, and hematite, and minor anhydrite, calcite, and apatite. Wenlanzhangite–(Y) occurs in the lower part of the bedded/massive orebody, and associated minerals are chalcopyrite, bornite, nolanite, thortveitite, jingwenite–(Y), and roscoelite (Fig. 3a). Wenlanzhangite–(Y) is observed as a dark brown, 70–100 μm–thick rim on a core domain of jingwenite–(Y) or 100 μm–thick core on jingwenite–(Y), which occurs as 100–200 μm columnar crystals (Fig. 3b–d). The crystals display regular oscillatory compositional zoning on back–scattered electron images (Fig. 3b).

ANALYTICAL METHODS

Reflectance measurements

Reflectance values for wenlanzhangite-(Y) were measured in air using a CRAIC 20/30PV Pro microspectrophotometer at Westlake University, Hangzhou, China. The reference material is aluminum metal (R= 85-90 %) (SPFS) with MgF_2 coating. Reflectance values were obtained from five spots in a single wenlanzhangite-(Y) grain, with × 50 objective and 16 × 16 μm aperture size.

Chemical composition analysis

Quantitative major–element analysis was performed at Xi'an Center of Mineral Resources Survey, China, using a Shimadzu EPMA–1720HT electron microprobe. All measurements were performed

using an accelerating voltage of 15 kV and a beam current of 50 nA. The beam size was 20 μm for the standards and 5 μm for wenlanzhangite-(Y). Crystals used were PET (Y, Sc and Si), LIF (Ce, Pr, Nd, Sm, Gd, Tb, Dy, Ho, Er, Tm, Yb and V), and RAP (Al). The *K*α line was chosen for analysis of Si, Al, V, and Sc; the *L*α line for Ce, Pr, Sm, Nd, Tb, Gd, Dy, Er, Yb, and Y; and the *L*β line for Ho and Tm. Count times on peaks were 10 s and background intensities were measured on both sides of the peak for half of the peak time. The standards were CeP_5O_{14} for Ce, PrP_5O_{14} for Pr, NdP_5O_{14} for Nd, SmP_5O_{14} for Sm, GdP_5O_{14} for Gd, $Tb_3Ga_5O_{12}$ for Tb, DyP_5O_{14} for Dy, HoP_5O_{14} for Ho, ErP_5O_{14} for Er, TmP_5O_{14} for Tm, YbP_5O_{14} for Yb, Y_2SiO_5 for Y and Si, kyanite for Al, YVO_4 for V and pure Sc for Sc. Element mapping was carried out using a JEOL JXA–8230 electron microprobe at the State Key Laboratory of Continental Dynamics, Northwest University (China), with an accelerating voltage of 15 kV, beam current of 50 nA and beam diameter of 2 μm.

In–situ trace element analysis was undertaken at the State Key Laboratory of Continental Dynamics, Northwest University (China). An Agilent 7900 ICP–MS coupled with RESOlution M–50 193–nm ArF Excimer Laser Ablation system was used to analyze mineral chemical compositions on polished thin sections. He and Ar were mixed via a T–connector before entering the ICP. International standard reference materials NIST SRM 610, NIST SRM 612, and BCR–2G were used as external standards for calculations (Bao et al. 2016). The concentration of Si obtained by EPMA was used as the internal standard for trace element content calculations. Data processing was performed using ICPMSDataCal (Liu et al. 2008).

Crystal structure analysis

A transparent single crystal (0.02 × 0.015 × 0.01 mm) was cut from the polished section on a double–focused ion beam platform (TESCAN GAIA 3). This crystal was used for the subsequent X–ray diffraction study. X–ray powder and single–crystal diffraction were carried out at the Science Research Institute, China University of Geosciences, China, with a Rigaku Oxford diffraction XtaLAB PRO–007HF single crystal diffractometer equipped with a rotating anode microfocus X–ray

source (50 kV, 24 mA; Mo$K\alpha$, λ = 0.71073 Å) and a hybrid pixel array detector. The crystal structure determination and refinement process of wenlanzhangite–(Y) were performed using OLEX2–1.3 (Dolomanov et al. 2009). The structure model was solved with the SHELXT using intrinsic phasing and refined by SHELXL with least square (Sheldrick 2015a, b). Since the crystal cell parameters obtained by X–ray single crystal diffraction were close to a monoclinic cell and different from those of jingwenite–(Y), selected–area electron diffraction (SAED) analyses for wenlanzhangite–(Y) were undertaken to confirm the single crystal data. Experiments were performed using a JEM–2100 (HR) Transmission Electron Microscope equipped with a double–tilt holder, a Gatan digital camera, and an INCA Energy TEM100 energy–dispersive spectroscopy instrument at the Institute of Mineral Resources, Chinese Academy of Geological Sciences, Beijing, operated at 200 kV. A TEM foil of about 50 nm thickness was prepared on a FIB–SEM platform (TESCAN GAIA 3) at the analytical laboratory of the Beijing Research Institute of Uranium Geology. Images of the foil and its location in polished section before cutting are shown in Fig. 3b. Results were successfully indexed with *P*–1 model and the calculated parameters are listed below.

Raman spectroscopy analysis

Raman spectra of wenlanzhangite–(Y) were collected from a randomly oriented grain using a Renishaw Invia confocal Raman spectrometer equipped with 50× objective at the State Key Laboratory of Continental Dynamics, Northwest University, Xi'an, China. Raman spectra were collected with an invia laser Raman spectrometer (Renishaw, UK) at 24 ℃. The excitation wavelength is 514.5 nm (semiconductor laser), and the output power of the laser was set at 100 mW with a Renishaw edge filter. The 50X objective on a Leica DM LM microscope was used, and a grating with 1800 grooves/mm was selected. The spectral resolution (apparatus function) was ~3.0 cm^{-1} determined by an emission spectrum from a neon lamp at ~918.6 cm^{-1}.

RESULTS

Optical, morphological, and physical properties of wenlanzhangite–(Y)

Wenlanzhangite-(Y) is translucent to transparent. Reflectance data are given in Table 1 and Figure 4. The refractive index n of wenlanzhangite–(Y) is 2.17, which is calculated by N=Kd+1 (K values from Mandarino 1981). The dispersion is medium with r<v, and the pleochroism is with X = brown, Y = dark brown, Z = brown black. The a: b: c ratio from single–crystal X–ray diffraction data is 0.601: 0.968: 1. The colour, streak, lustre, and hardness (Mohs) are dark brown, yellow grey, vitreous, and ~4, respectively. The cleavage is good and parallel to {110}. The calculated density is 4.54 g/cm^3 based on the empirical formula and unit cell volume determined from single crystal XRD data.

Chemical composition

Wenlanzhangite-(Y) displays narrow ranges of SiO_2, Al_2O_3,Y_2O_3, Dy_2O_3, Er_2O_3, Gd_2O_3, Yb_2O_3, Nd_2O_3, and Sm_2O_3 contents, ranging from 16.07 to 16.63 wt%, 3.38 to 4.18 wt%, 18.55 to 19.59 wt%, 3.93 to 4.46 wt%, 2.42 to 3.11 wt%, 1.88 to 2.34 wt%, 2.18 to 2.74 wt%, 1.86 to 2.27 wt%, and 1.16–1.48 wt%, respectively. Sc_2O_3, Ho_2O_3, Ce_2O_3, Tb_2O_3, Tm_2O_3, and Pr_2O_3 contents are low with 0.15–0.66 wt%, 0.54–1.11 wt%, 0.26–0.50 wt%, 0.45–0.67 wt%, 0.38–0.80 wt%, and 0.08–0.28 wt%, respectively (Table 2). The average empirical formula, calculated on the basis of 8 cations per formula unit (apfu), is $(Y_{1.26}Dy_{0.17}Er_{0.11}Gd_{0.09}Yb_{0.09}Nd_{0.09}Sm_{0.06}Sc_{0.04}Ho_{0.03}Ce_{0.02}Tb_{0.02}Tm_{0.02}Pr_{0.01})_{\Sigma 2.00}(V^{3+}_{1.46}Al_{0.54})_{\Sigma 2.00}V^{4+}_2(SiO_4)_2O_4(OH)_4$. The type and amount of OH were determined from bond–valence calculations of O atoms in the crystal structure, and the Raman spectrum of wenlanzhangite–(Y) (Fig. 5). As for total REE and HREE contents, wenlanzhangite–(Y) has ∑REE concentrations of 2.50–2.98×10^5 ppm, with Y/Ho ratios (16–19, mean= 18), and Eu/Eu* (0.21–0.32, mean= 0.26) ratios (Fig. 6; Table S1).

Crystal structure

Unit–cell parameters obtained from the single–crystal and selected–area electron using TEM diffraction (Fig. 7) data are: a = 5.9632(7) Å, b = 9.599(1) Å, c = 9.9170(9) Å, α = 90.033(8)°, β = 98.595(2)°, γ = 90.003(9)°, and V = 561.28(10) Å^3, and a = 5.948(1) Å, b = 9.616(1) Å, c = 9.916(1) Å, α = 90.00(1)°, β = 98.35(1)°, γ = 90.00(1)°, and V = 561.14(3) Å^3, respectively. The X–ray

powder diffraction data are shown in Table S2. The initial crystal structure determination was performed using OLEX2–1.3 (Dolomanov et al. 2009), and the refined structure model was solved with the SHELXT2014/5 directly and subsequently by SHELXL2016/6 with least square refinement (Sheldrick 2015a, b). Although the single–crystal XRD data indicate two possible crystal structures, *P*–1 and *I*2/a, the TEM results indicated that the SAED can only be indexed by a *P*–1 structure and not *I*2/a. The structure was therefore solved in space group *P*–1 (#2). Crystallographic data and refinement statistics are given in Table 3. The occupancies of atoms are refined toward minimum R_1 and show good agreement with the measured chemical composition. For simplicity, only Y and Dy are considered in the refinement for rare earth elements (REE), since they are the first two major elements according to microprobe analyses. The final atomic coordinates and displacement parameters are listed in Table 4, and selected bond lengths in Table 5. The bond–valence sums of atoms are presented in Table S3.

The structure of wenlanzhangite–(Y) is composed of *a*–axis–oriented chains of edge-sharing [VO_6] octahedra linked by insular [SiO_4] tetrahedra, leaving open channels occupied by rare earth elements (Fig. 8). The octahedra could be divided into two types according to geometry. Type one ([$V1O_6$] and [$V2O_6$]) are strongly distorted octahedra (DO) with respect to the major difference between the shortest V–O distance (≈1.7 Å) and the longest V–O distance (≈2.4 Å). Type two ([$V3O_6$], [$V4O_6$] and [$V5O_6$]) are closer to regular octahedra (RO). Two different octahedra are distributed in different chains, respectively. Like the structure of jingwenite-(Y) (Liu et al. 2023), the two types are dominated by V^{4+} in [$V1O_6$] and [$V2O_6$], and by V^{3+} in [$V3O_6$], [$V4O_6$] and [$V5O_6$] for wenlanzhangite-(Y). The [SiO_4] tetrahedra share corners with two separate chains of RO and share corners with two neighboring octahedra in the same chains of DO. Rare earth elements are 8–coordinated and occupy open channels along the *b*–axis. Bond valence calculations show that hydrogen atoms are attached with four oxygen atoms (O13, O14, O15, O16), leading to the ideal crystal chemical formula $Y_2V^{3+}{}_2V^{4+}{}_2(SiO_4)_2O_4(OH)_4$. The atomic occupancies for each site are

195 described below:

196 **(1) V1 and V2 sites**: These two sites are 6–coordinated. The bond valence calculations of
197 jingwenite–(Y) (Liu et al. 2023) have indicated that a similar site is dominated by V^{4+}. This situation
198 is consistent in wenlanzhangite-(Y). But, during the structure refinement of wenlanzhangite–(Y),
199 slightly weaker scatterers of X–rays than V are noticed at both sites, indicating that some
200 heterovalent Al^{3+} can co–occupy the V1 and V2 sites. This is also confirmed by broadband
201 viscoelastic spectroscopy. The edge–sharing chains of $[V^{4+}O_6]$ octahedra also occur in synthetic VO_2
202 (C2/m) (Marezio et al. 1972) and VO_2 ($P2_1/c$) (Longo and Kierkegaard 1970), in which V–O bond
203 lengths vary from 1.73 Å to 2.13 Å.

204 **(2) V3, V4 and V5 sites:** These three sites are 6–coordinated. V^{3+} and Al^{3+} are mixed in **V5**
205 sites and structure refinement result shows they are all dominated by V^{3+}.

206 **(3) Si sites:** there are two distinct Si positions, all tetrahedrally coordinated by oxygen anions.
207 The average Si–O distances are 1.654 and 1.650 Å, which is longer than the normally observed range
208 in silicates.

209 **(4) REE sites:** Y1 and Y2 sites are 8–coordinated and dominated by Y^{3+}. Dy3 and Dy4 sites are
210 dominated by □, because they only possess 7.34 and 7.28 e^-. They are recognized as trace amounts
211 of Dy^{3+} rather than Y^{3+} due to the average bond length of Dy3–O being longer than either Y1–O or
212 Y2–O. The small amounts of additional rare earths balance the valence state that is insufficient due
213 to the substitution of Al^{3+} for tetravalent elements (e.g., V^{4+}).

214 Therefore, the crystal structure of wenlanzhangite–(Y) is sufficiently close to that of
215 jingwenite–(Y) (Liu et al. 2023) that it should be classified within the same group of jingwenite–(Y)
216 with a Dana classification number 52.4.10.2.

217 **Raman spectrum**

218 The Raman spectrum of wenlanzhangite–(Y) shows the bands of O–H stretching vibrations at 3572
219 cm^{-1}, the bands of Si–O stretching vibrations at 829, 893, and 951 cm^{-1}, and the bands of Al–O, V–O,

and Y–O vibrations in the range of 100–600 cm^{-1} (Liu et al. 2023).

DISCUSSION

In contrast to jingwenite–(Y) with 21.65 wt% VO_2, 4.04 wt% V_2O_3, and 10.85 wt% Al_2O_3, wenlanzhangite–(Y) displays similar VO_2 (22.05–22.60 wt%) but higher V_2O_3 (14.07–15.42 wt%) and lower Al_2O_3 (3.38–4.18 wt%) contents. Moreover, the crystal system, space group, and unit cell of wenlanzhangite–(Y) are all distinct from those of jingwenite–(Y) (Table 6) (Fig. 8). The structure of jingwenite–(Y) is composed of *b*–axis–oriented chains of octahedra consisting of edge–sharing Al (V, Fe)–O octahedra and V (Ti)–O octahedra linked by insular Si–O tetrahedra (Liu et al. 2023). In the chains of Al–O octahedra, two alternative cation sites, Al1 and Al2, share edges O4–O4 and O7–O7. Both sites are dominated by Al but with the incorporation of Fe^{3+} and V^{3+}, more in Al2 than in Al1. On this basis, V mainly occurs as V^{4+} in jingwenite–(Y), while V^{3+} can substitute for Al^{3+} and Fe^{3+}. Both V^{3+} and V^{4+} are dominant cations in wenlanzhangite–(Y) with less Al^{3+} and Fe^{3+}. The differences in space group and unit cell are the results of the splitting of V sites. Given the measured variation in calculated $V^{3+}/(V^{3+}+Al)$, there is likely a solid–solution series extending from endmember, $Y_2Al_2V^{4+}{}_2(SiO_4)_2O_4(OH)_4$, toward another endmember, $Y_2V^{3+}{}_2V^{4+}{}_2(SiO_4)_2O_4(OH)_4$. Compositions across this solid solution are present in the zoned crystal shown in Fig. 3b, in which $V^{3+}/(V^{3+}+Al+Fe^{3+})$, ranges from 0.19 in jingwenite–(Y) up to 0.76 (equivalent to 1.53 a.p.f.u. V^{3+}) in wenlanzhangite–(Y) (Fig. 6b) (Tables 4 and S1). The observed intracrystal zoning is likely an expression of an evolutionary process involving changes in the composition of hydrothermal fluid and/or fluid parameters over time. Moreover, the structure of a V–enriched analogue of jingwenite–(Y), $Y_2AlV^{3+}V^{4+}{}_2(SiO_4)_2O_4(OH)_4$, has been determined in which the two nearly regular octahedra sites are dominated by Al^{3+} and V^{3+}, respectively.

IMPLICATIONS

In general, V can be dissolved and transported in oxidized fluids as V^{5+}. In turn, V^{4+} and V^{3+} are

insoluble in hydrothermal fluids and preferentially partition into mineral phases (Fischer 1973; Huang et al. 2015b). Thus, like HREE and U, V is also likely leached and transported as V^{5+} by oxidized fluids, and then reduced to insoluble V^{4+} or V^{3+} upon contact with organic– and apatite–rich beds in the overlying dolostone/limestone, precipitating and partitioned into jingwenite–(Y). The presence of wenlanzhangite–(Y) as rims on normal jingwenite–(Y) indicates an evolution to a relatively more reduced hydrothermal environment causing conversion, in which V^{5+} is reduced to V^{4+} and additional V^{3+}. This interpretation is also suggested by the higher Eu/Eu* ratios in wenlanzhangite–(Y) (Fig. 6c), as well as by the negative correlation between measured Fe^{3+} and calculated V^{3+}. Dissolution of Fe–Mn–rich particles or oxyhydroxides can lead to fractionation of Y and Ho due to the higher marine particle–reactivity of Ho compared to Y (Bau et al. 1996). Fe–Mn oxyhydroxides facilitate dissolution under anoxic conditions, yielding low Y/Ho ratios (<28) in hydrothermal systems (Planavsky et al. 2010). Therefore, the lower Y/Ho ratios in wenlanzhangite–(Y) (Fig. 6c) can be interpreted as a response to greater volumes of Fe–Mn–rich oxyhydroxides in dolostone/limestone and red sandstone dissolved in relatively reduced ore–forming fluids during fluid–rock reaction. All these observations suggest that wenlanzhangite–(Y) and jingwenite–(Y) have great potential as proxies for tracing the redox state of ore–formation. Temperature and pressure conditions of wenlanzhangite-(Y) formation are estimated to be 110–287 °C and 50 MPa, respectively, based on fluid-inclusion studies (Liu 1997; Jiang et al. 2016).

ACKNOWLEDGMENTS

This research was jointly funded by the National Natural Science Foundation of China (grants 42272070, 42130102, 42242201, and 42102080), the Young Star of Science and Technology Plan Projects in Shaanxi Province, China (Grant 2023KJXX–037) and the Natural Science Basic Research Program in Shaanxi Province of China (2022JC–DW5–01). The authors thank Dr. Yuan Cheng, Instrumentation and Service Center for Molecular Sciences, Westlake University, for the reflectance measurement. We are grateful to the editors Don Baker and Paolo Lotti, and two anonymous

reviewers for their constructive and critical comments and suggestions.

REFERENCES

Bao, Z.A., Yuan, H.L., Zong, C.L., Liu, Y., Chen, K.Y., and Zhang, Y.L. (2016) Simultaneous determination of trace elements and lead isotopes in fused silicate rock powders using a boron nitride vessel and fsLA–(MC)–ICP–MS. Journal of Analytical Atomic Spectrometry, 31, 1012.

Bau, M., Koschinsky, A., Dulski, P., and Hein, J.R. (1996) Comparison of the partitioning behaviours of yttrium, rare earth elements, and titanium between hydrogenetic marine ferromanganese crusts and seawater. Geochimica et Cosmochimica Acta, 60, 1709–1725.

Chen, M.H., Ke, C.H., Tian, Y.F., Chen, G., Ma, K.Z., Ma, S.X., Peng, Y.X., and Zhang, W. (2021) Sedimentary–exhalative massive sulfide deposits in shallow marine environment: a case study from Yushui copper deposit, Guangdong Province. Acta Geologica Sinica, 95, 1774–1791 (in Chinese with English abstract).

Dahlkamp, F.J. (2010) Uranium deposits of the world–USA and Latin America. Berlin, Germany, Springer, 423 p.

Dolomanov, O.V., Bourhis, L.J., Gildea, R.J., Howard, J., and Puschmann, H. (2009) Olex2: a complete structure solution, refinement and analysis program. Journal of Applied Crystallography, 42, 339–341.

Fischer, R.P. (1973) Vanadium. In Brobst, D.A., and Pratt, W.P., Eds., United States Mineral Resources: U.S. Geological Survey Professional Paper, 820, 679–688.

Huang, Y., Sun, X.M., Shi, G.Y., Sa, R.N., Guang, Y., Jiang, X.D., and Que, H.H. (2015a) Re–Os dating of sulfides from the Yushui Cu–polymetallic deposit in eastern Guangdong Province, South China. Ore Geology Reviews, 70, 281–289.

Huang, J.H., Huang, F., Evans, L., and Glasauer, S. (2015b) Vanadium: Global (bio) geochemistry. Chemical Geology, 417, 68–89.

Jiang, B.B., Zhu, X.Y., Cheng, X.Y., Wang, H. (2016) Characteristics and geological significance of

294 fluid inclusions in the Yushui copper polymetallic deposit, Guangdong Province. Geology in
295 China 43, 2163–2172 (in Chinese with English abstract).
296 Liu, J.Q. (1997) Thermobarogeochemistry, ore-forming age and genesis study for the Yushui
297 copper-rich multimetal deposit in Meixian county, Guangdong Province, Southern China.
298 Geology and Mineral Resources of South China, 1, 37-50 (in Chinese with English abstract)
299 Liu, P., Gu, X.P., Zhang, W.L., Hu, H., Chen, X.D., Wang, X.L., Song W.L., Yu, M., and Cook, N.J.
300 (2023) Jingwenite–(Y) from the Yushui Cu deposit, South China: the first occurrence of a V–
301 HREE–bearing silicate mineral. American Mineralogist, 108–196.
302 Liu, Y.S., Hu, Z.C., Gao, S., Liu, Y.S., Hu, Z.C., Gao, S., Günther, D., Xu, J., Gao, C.G., and Chen,
303 H.H. (2008) In situ analysis of major and trace elements anhydrous minerals by LA–ICP–MS
304 without applying an internal standard. Chemical Geology, 257, 34–43.
305 Longo, J.M., and Kierkegaard, P. (1970) A refinement of the structure of VO2. Acta Chemica
306 Scandinavica, 24, 420–426.
307 Mandarino, J.A. (1981) The Gladstone–Dale relationship: Part IV, The compatibility concept and its
308 application. The Canadian Mineralogist, 19, 441–450.
309 Marezio, M., McWhan, D.B., Remeika, J.P., and Dernier, P.D. (1972) Structural aspects of the
310 metal–insulator transition in Cr–doped VO2. Physical Review B: Solid State,5, 2541–2551.
311 Momma, K., and Izumi, F. (2011) VESTA 3 for three–dimensional visualization of crystal,
312 volumetric and morphology data. Journal of Applied Crystallography, 44, 1272–1276.
313 Northrop, H.R., Goldhaber, M.B., Landis, G.P., Unruh, J.W., Reynolds, R.L., Campbell, J.A., Wanty,
314 R.B., Grauch, R.I., Whitney, G., and Rye, R.O. (1990) Genesis of the tabular–type vanadium–
315 uranium deposits of the Henry basin, Utah. Economic Geology, 85, 215–269.
316 Planavsky, N., Bekker, A., Rouxel, O.J., Kamber, B., Hofmann, A., Knudsen, A., and Lyons, T.W.
317 (2010) Rare earth element and yttrium compositions of Archean and Paleoproterozoic Fe
318 formations revisited: new perspectives on the significance and mechanisms of deposition.

319 Geochimica et Cosmochimica Acta, 74, 6387–6405.
320 Shawe, D.R. (2011) Uranium–vanadium deposits of the Slick Rock district, Colorado. U.S.
321 Geological Survey Professional Paper, 576–F, 67.
322 Sheldrick, G.M. (2015a) SHELXT–Integrated space–group and crystal structure determination. Acta
323 Crystallographica, A71, 3–8.
324 Sheldrick, G.M. (2015b) Crystal structure refinement with SHELX. Acta Crystallographica, C71, 3–
325 8.
326 Weeks, A.D., Coleman, R.G., and Thompson, M.E. (1959) Summary of the ore mineralogy, part 5 of
327 Garrels, R.M., and Larsen, E.S. III, comps., Geochemistry and mineralogy of the Colorado
328 Plateau uranium ores (3rd ed.). U.S. Geological Survey Professional Paper, 320, 65–79.

FIGURE CAPTIONS

Fig 1. (a) Geological map of the Yushui deposit (after Huang et al., 2015a). (b) Geological cross section of the exploration line a–b (from Chen et al., 2021).

Fig 2. (a) Stratigraphic column of the Yushui deposit. (b) Photograph of drillcore of red sandstone; (c)–(e) Photographs of bedded orebody. (f) Photomicrograph of disseminated ore in red sandstone. (g) Photograph of vein–style orebody in red sandstone. Bn–bornite; Cc–chalcocite; Ccp–chalcopyrite.

Fig 3. Photomicrographs showing the occurrence and mineral association of wenlanzhangite–(Y) and jingwenite–(Y) (Jw–Y). (a). Wenlanzhangite–(Y) (Wlz–Y) as a dark brown, 100 μm–thick core on jingwenite–(Y) with bornite (Bn), roscoelite (Rcl), and thortveitite (Tv). (b) Back–scattered electron image of euhedral jingwenite–(Y) and wenlanzhangite–(Y) crystals with bornite, in reflected light, parallel nicols. (c) and (d). EPMA element (Al and V) maps of the marked box shown in (b). Note grain–scale compositional zoning in (b) reflecting variation from typical jingwenite–(Y), $Y_2Al_2V^{4+}_2(SiO_4)_2O_4(OH)_4$, to wenlanzhangite–(Y).

Fig 4. Reflectance data for wenlanzhangite–(Y) in air. The reflectance values (R%) are plotted versus wavelength in nm.

Fig 5. Raman spectra for wenlanzhangite–(Y).

Fig 6. (a). Chondrite–normalized rare earth element (REE) fractionation patterns for jingwenite–(Y) and wenlanzhangite–(Y). (b). Y/(REE+Y+Sc) vs. $V^{3+}/(V^{3+}+Al+Fe^{3+})$ ratio plot. (c). Eu/Eu* vs. Y/Ho ratio plots for jingwenite–(Y) and wanlanzhangite–(Y).

Fig 7. SAED patterns of wenlanzhangite–(Y) from 4 different zone axes.

Fig 8. Crystal structure of wenlanzhangite–(Y) (a) and jingwenite–(Y) (b), plotted with VESTA (Momma and Izumi, 2011).

This is the peer-reviewed, final accepted version for American Mineralogist, published by the Mineralogical Society of America.
The published version is subject to change. Cite as Authors (Year) Title. American Mineralogist, in press.
DOI: https://doi.org/10.2138/am-2023-9220. http://www.minsocam.org/

352 # TABLE CAPTIONS

353 **Table 1.** Reflectance data for wenlanzhangite–(Y).

354 **Table 2.** Major–element data for wenlanzhangite–(Y) compared with jingwenite–(Y) (wt.%).

355 **Table 3**. Information on crystal and structural refinement for wenlanzhangite–(Y).

356 **Table 4.** Site, Wyckoff position (*W.p.*), site occupancy (s.o.), fractional atomic coordinates, and

357 equivalent isotropic (and anisotropic) displacement parameters ($Å^2$) for wenlanzhangite–(Y).

358 **Table 5.** Selected bond lengths (Å) for wenlanzhangite–(Y).

359 **Table 6.** Comparison between wenlanzhangite–(Y) and jingwenite–(Y).

360 # SUPPLEMENTARY TABLE CAPTIONS

361 **Table S1** REE contents in jingwenite–(Y) and wenlanzhangite–(Y) as determined by LA–ICP–MS.

362 **Table S2**. X-ray powder diffraction data (*d* in Å, *I* in %) for wenlanzhangite-(Y).

363 **Table S3.** Calculated bond valences (*v.u.*) for atoms in wenlanzhangite-(Y).

364

116° 10′ 40″
116° 10′ 54″
116° 11′ 08″
24° 25′ 25″
24° 25′ 09″
(a)
Mongolia
Beijing
South China
Yushui
N
b
a
Fig. 1b
0
100 m
Quaternary alluvium
Middle-Upper Devonian clastic rocks
Lower Cretaceous volcanic rocks of the Guancaohu Formation
Granite porphyry (zircon U-Pb age: 128 ± 1 Ma, Li et al., 2019)
Upper Jurassic volcanic rocks of the Gaojiping Formation
Dolerite (zircon U-Pb age: 59 ± 3 Ma, Li et al., 2019)
Upper Carboniferous limestone and dolomite of the Hutian Formation
Fault
Lower Carboniferous red sandstone of the Zhongxin Formation
Ore body
(b)
a
b
elevation (m)
150
100
50
0
-50
-100
-150
ZK0-1
ZK1-2
ZK4-6
V_1
Fig. 2a
0
100m

Fig. 1 revision 2

(a)

Vein-type ore

Upper part

Bedded orebody

Lower part

Disseminated ore

B

C

D

E

F

G

10 m

Dolomite/limestone

Sandstone

(b) Red sandstone

(c) Ccp

(d) Bn

(e) Cc

(f) Red sandstone

Ccp

Vein orebody

(g) Sandstone

Ccp

200 μm

Fig. 2 revision 2

(a)
Jw-Y
Jw-Y
Jw-Y
Wlz-Y
Tv
Nol
Rcl
100 μm
(b)
Jw-Y
Jw-Y-7
Jw-Y-10
Wlz-Y-5
Wlz-Y-7
Bn
Jw-Y-1
Jw-Y
FIB foil
Jw-Y-6
Wlz-Y-1
Fig. 3c, d
Wlz-Y-4
50 μm
(c)
Laser spot
Al
50 μm
(d)
V
High
Low
50 μm

Fig. 3 revision 2

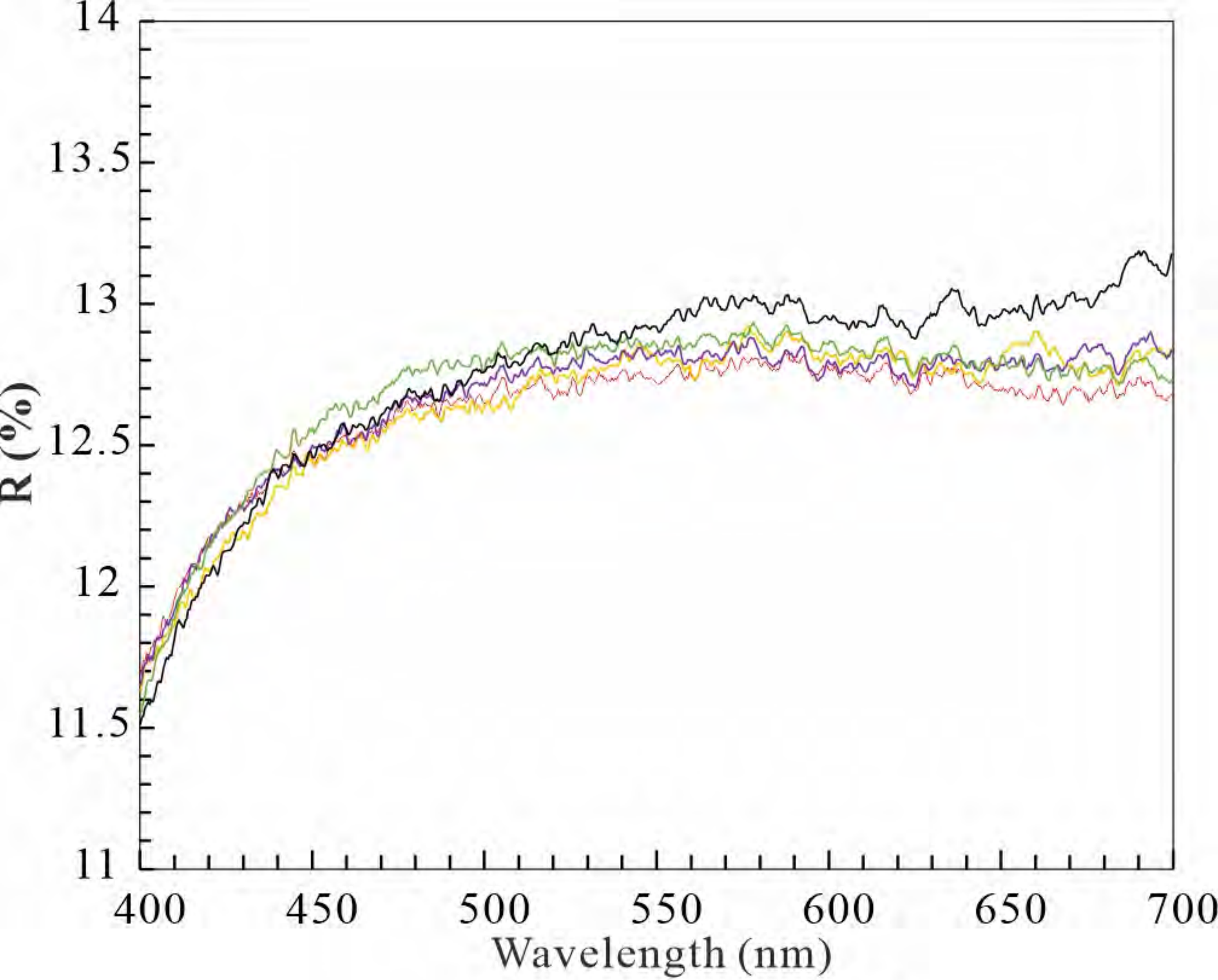

Fig. 4 revision 2

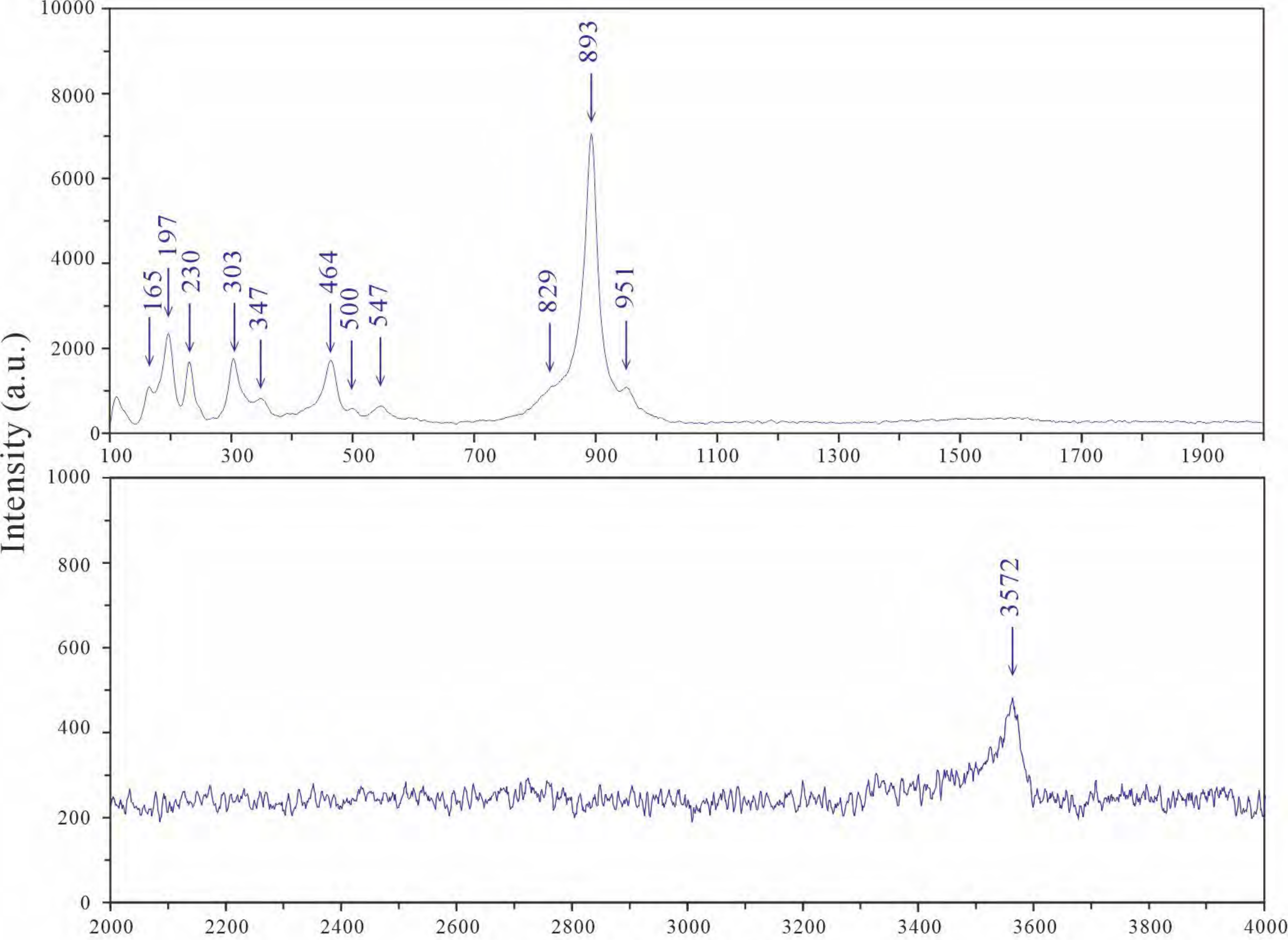

Fig. 5 revision 2

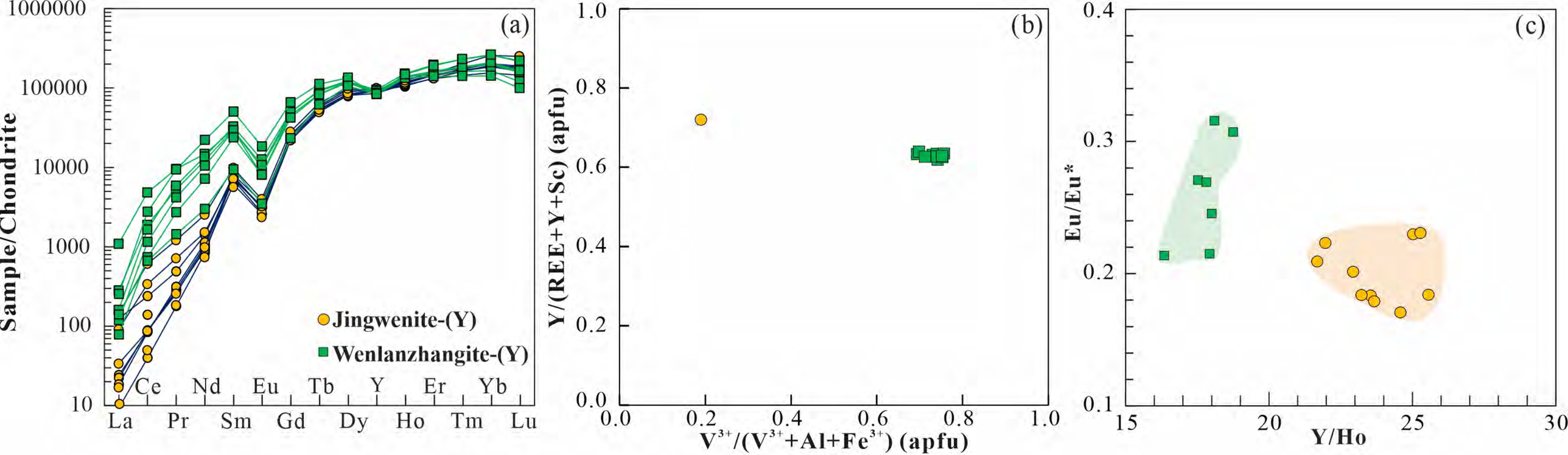

Fig. 6 revision 2

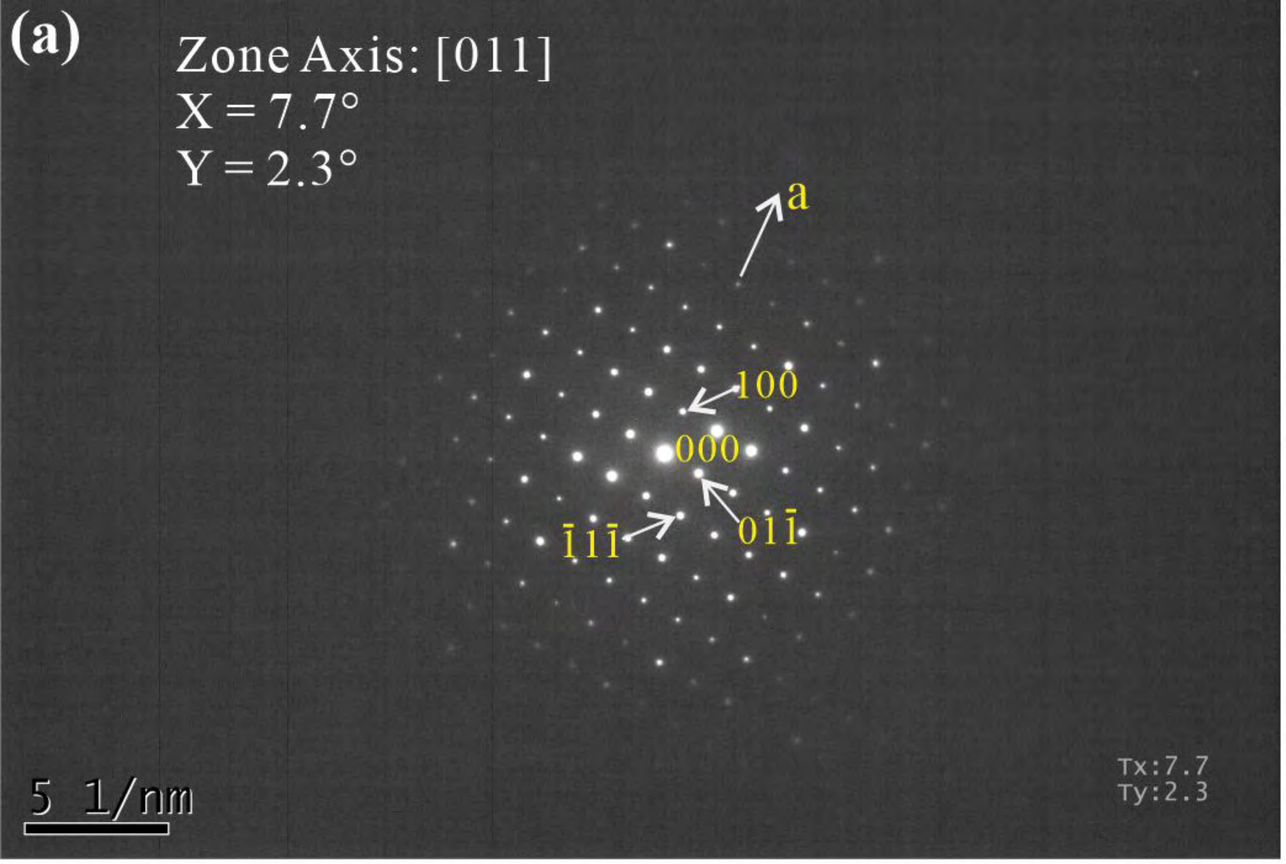

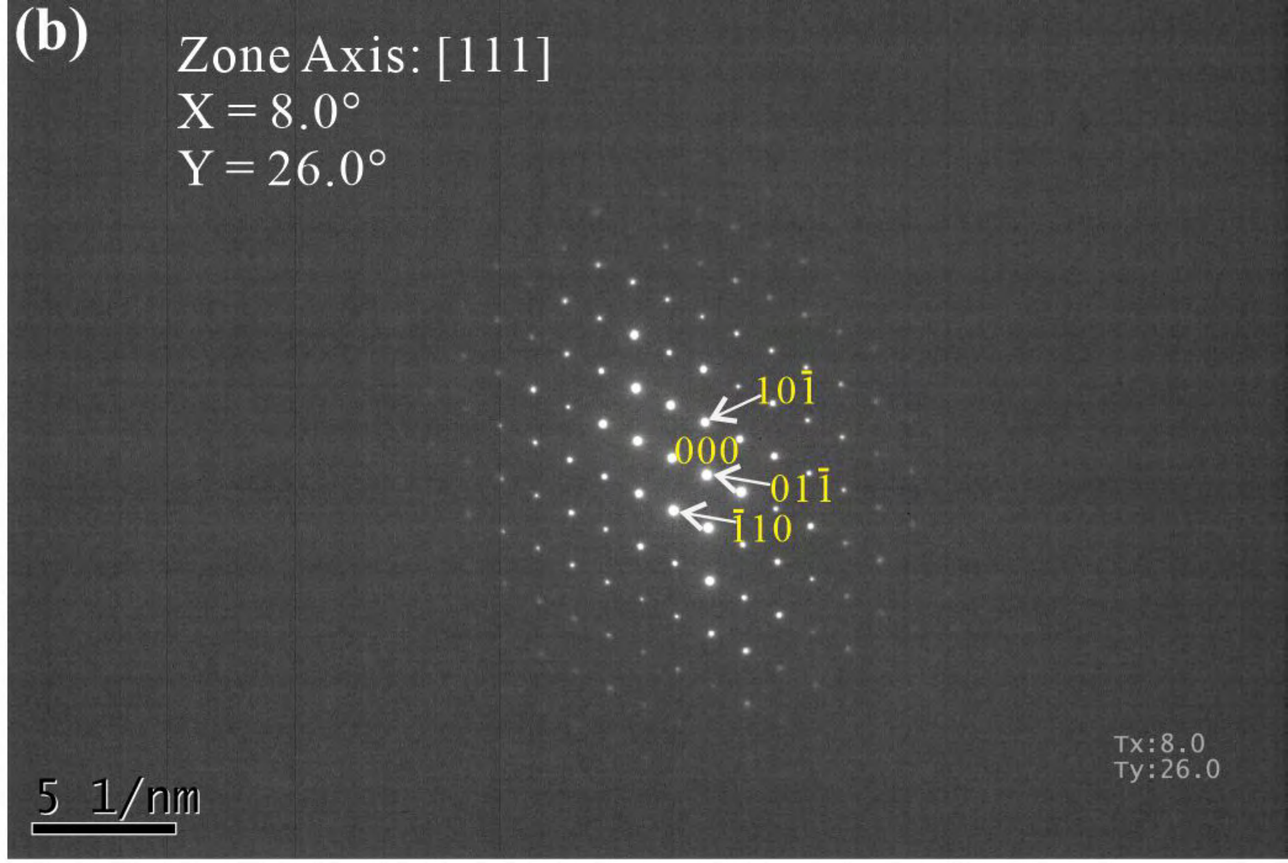

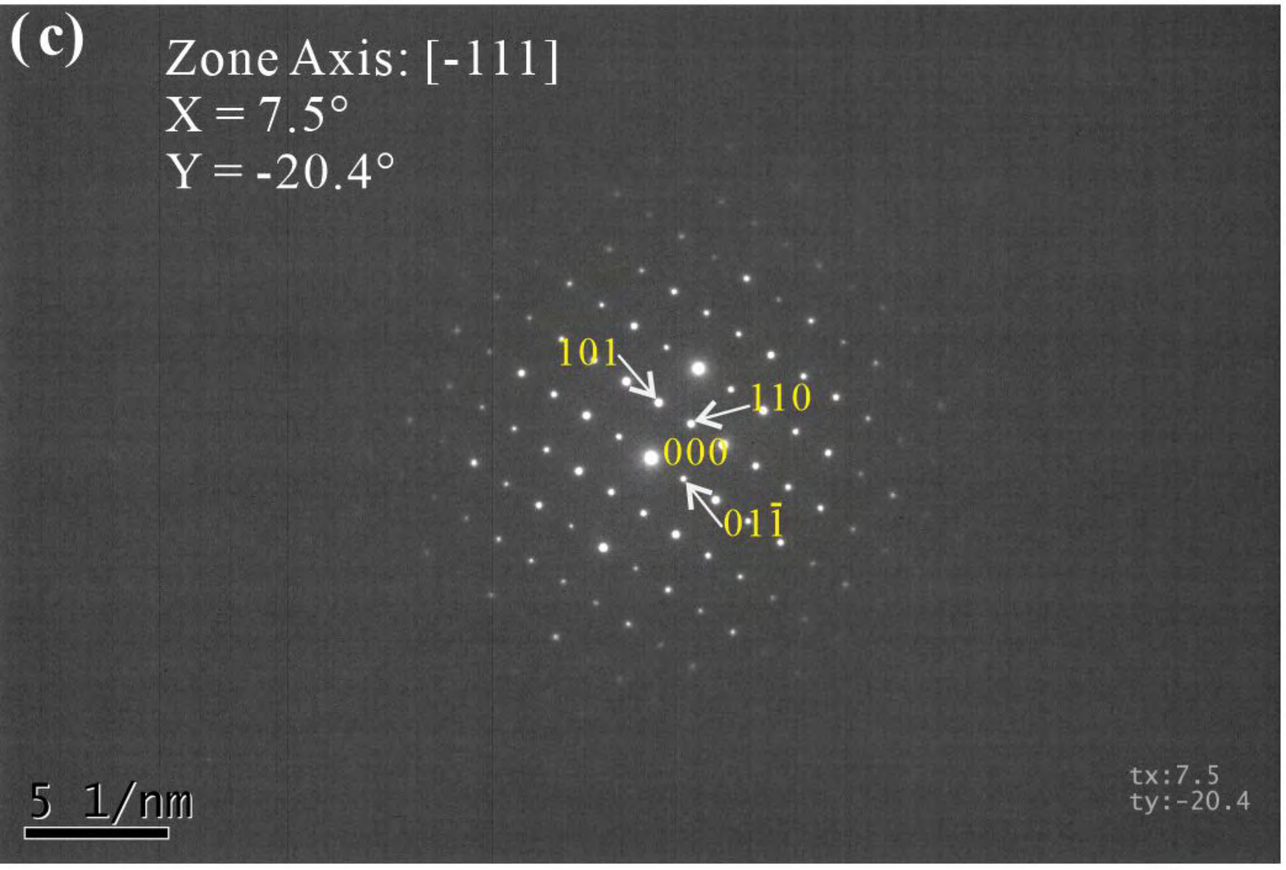

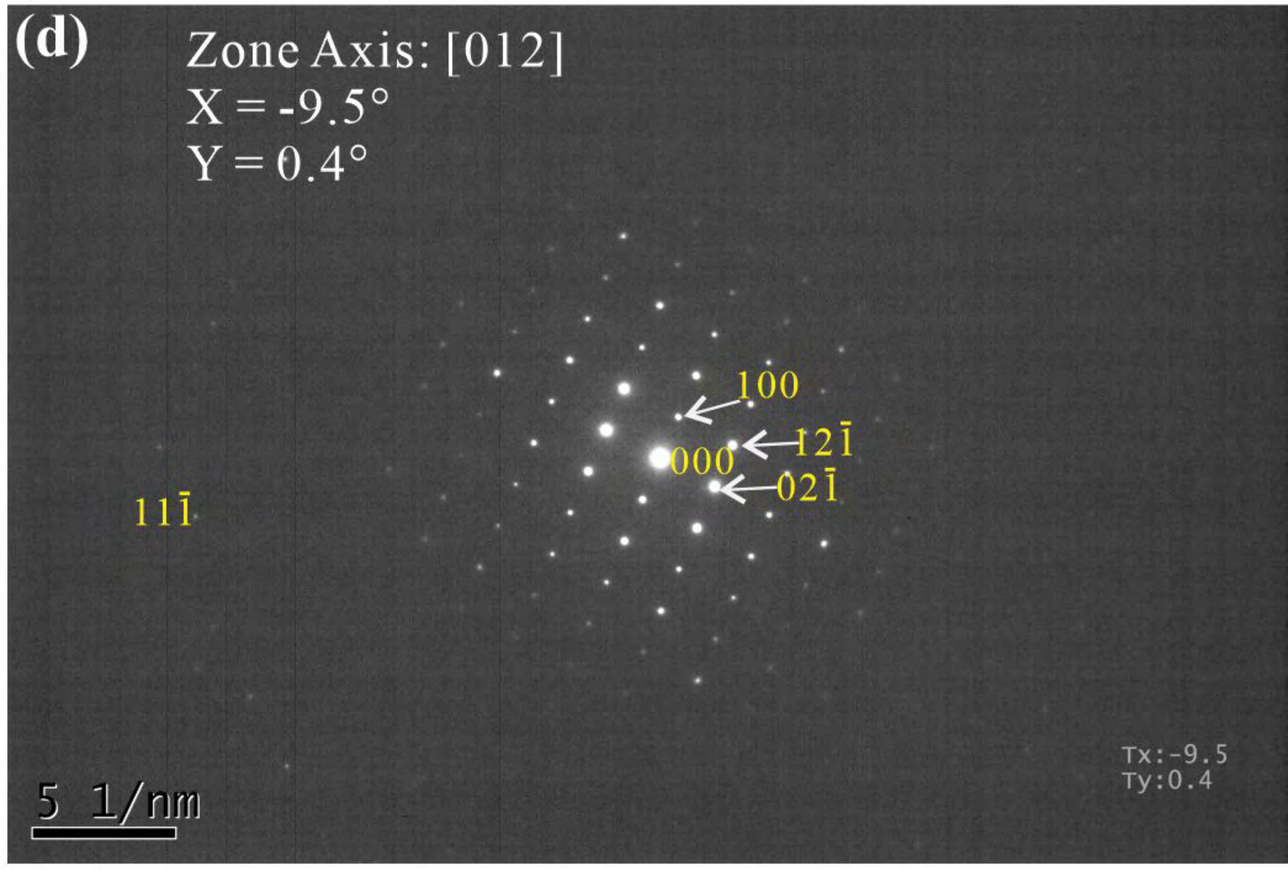

Fig. 7 revision 2

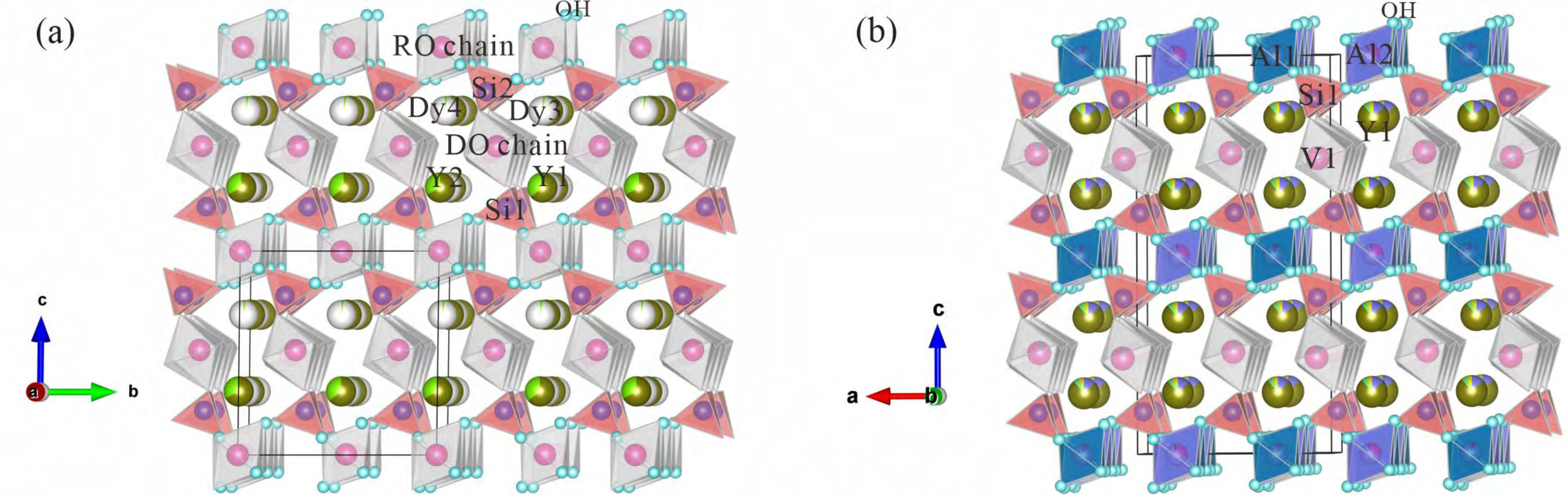

Fig. 8 revision 2

Table 1. Reflectance data for wenlanzhangite–(Y).

λ (nm)	R_{max} (%)	R_{min} (%)
400	11.7	11.5
420	12.2	12.0
440	12.5	12.4
460	12.6	12.5
470	**12.7**	**12.5**
480	12.8	12.6
500	12.8	12.6
520	12.8	12.7
540	12.9	12.8
546	**12.9**	**12.8**
560	13.0	12.8
580	13.0	12.8
589	**13.0**	**12.9**
600	12.9	12.8
620	12.9	12.7
640	13.0	12.7
650	**13.0**	**12.7**
660	13.0	12.7
680	13.0	12.7
700	13.2	12.7

Table 2. Major-element data for wenlanzhangite–(Y) compared with jingwenite–(Y) (wt.%). Number of point analyses = 10.

Constituent	Jw-Y	Wlz-Y-1	-2	-3	-4	-5	-6	-7	-8	-9	-10	Mean (Wlz-Y)
SiO_2	16.45	16.48	16.25	16.24	16.10	16.07	16.61	16.63	16.38	16.50	16.55	16.38
Al_2O_3	10.85	3.53	3.71	3.38	3.67	3.45	4.18	3.96	3.80	3.89	3.69	3.73
VO_2*	21.65	22.25	22.40	22.28	22.10	22.05	22.55	22.60	22.49	22.49	22.40	22.36
V_2O_3*	4.04	14.96	15.17	15.42	14.81	14.90	14.07	14.49	15.04	14.27	14.51	14.76
Fe_2O_3	0.89	<mdl	<mdl	<mdl	<mdl	<mdl	<mdl	<mdl	<mdl	<mdl	<mdl	<mdl
TiO_2	1.83	<mdl	<mdl	<mdl	<mdl	<mdl	<mdl	<mdl	<mdl	<mdl	<mdl	<mdl
Sc_2O_3	<mdl	0.34	0.20	0.19	0.21	0.15	0.66	0.62	0.21	0.65	0.46	0.37
Y_2O_3	24.67	18.55	19.12	19.13	19.04	18.92	19.30	19.55	19.45	19.59	19.26	19.19
Ce_2O_3	<mdl	0.50	0.33	0.39	0.26	0.42	0.33	0.38	0.35	0.31	0.36	0.36
Pr_2O_3	<mdl	0.14	0.17	0.08	0.20	0.19	0.13	0.23	0.12	0.28	0.19	0.17
Nd_2O_3	0.03	2.19	1.97	1.91	1.98	2.08	1.86	2.11	2.10	2.00	2.27	2.05
Sm_2O_3	0.1	1.38	1.27	1.21	1.26	1.16	1.40	1.51	1.26	1.41	1.48	1.33
Gd_2O_3	0.69	2.20	1.96	1.96	1.95	1.93	2.22	2.27	1.88	2.34	2.25	2.09
Tb_2O_3	0.32	0.45	0.59	0.51	0.59	0.67	0.58	0.49	0.63	0.49	0.57	0.56
Dy_2O_3	3.25	4.35	4.29	4.40	4.07	4.25	4.12	3.97	4.46	3.93	4.17	4.20
Ho_2O_3	0.83	0.61	0.71	0.67	0.85	1.11	0.68	0.54	0.54	0.83	0.67	0.72
Er_2O_3	3.55	2.80	3.08	3.03	3.02	3.11	2.61	2.42	3.03	2.60	2.55	2.83
Tm_2O_3	0.6	0.80	0.61	0.71	0.56	0.50	0.78	0.66	0.38	0.71	0.71	0.64
Yb_2O_3	3.99	2.24	2.74	2.70	2.60	2.55	2.34	2.18	2.60	2.20	2.22	2.44
Lu_2O_3	2.4	<mdl	<mdl	<mdl	<mdl	<mdl	<mdl	<mdl	<mdl	<mdl	<mdl	<mdl
H_2O*	4.65	4.83	4.87	4.84	4.80	4.79	4.90	4.91	4.89	4.89	4.87	4.86
Total	101.23	98.58	99.43	99.04	98.05	98.32	99.33	99.51	99.59	99.37	99.19	99.04
	apfu	Calculated on basis of 8 cations										
Sc	-	0.04	0.02	0.02	0.02	0.02	0.07	0.07	0.02	0.07	0.05	0.04
Y	1.54	1.22	1.25	1.26	1.27	1.26	1.26	1.27	1.27	1.28	1.26	1.26
Ce	-	0.02	0.01	0.02	0.01	0.02	0.01	0.02	0.02	0.01	0.02	0.02
Pr	-	0.01	0.01	0.00	0.01	0.01	0.01	0.01	0.01	0.01	0.01	0.01
Nd	0.00	0.10	0.09	0.08	0.09	0.09	0.08	0.09	0.09	0.09	0.10	0.09
Sm	0.00	0.06	0.05	0.05	0.05	0.05	0.06	0.06	0.05	0.06	0.06	0.06
Gd	0.02	0.09	0.08	0.08	0.08	0.08	0.09	0.09	0.08	0.10	0.09	0.09
Tb	0.02	0.02	0.02	0.02	0.02	0.03	0.02	0.02	0.03	0.02	0.02	0.02
Dy	0.12	0.17	0.17	0.18	0.16	0.17	0.16	0.16	0.18	0.16	0.17	0.17

Ho	0.04	0.02	0.03	0.03	0.03	0.04	0.03	0.02	0.02	0.03	0.03	0.03
Er	0.14	0.11	0.12	0.12	0.12	0.12	0.10	0.09	0.12	0.10	0.10	0.11
Tm	0.02	0.03	0.02	0.03	0.02	0.02	0.03	0.03	0.01	0.03	0.03	0.02
Yb	0.14	0.08	0.10	0.10	0.10	0.10	0.09	0.08	0.10	0.08	0.08	0.09
Lu	0.08	-	-	-	-	-	-	-	-	-	-	-
Total (Sc,Y,REE)	2.13	1.98	1.99	1.99	1.99	2.01	2.01	2.01	1.99	2.04	2.02	2.00
Al	1.5	0.52	0.54	0.49	0.54	0.51	0.60	0.57	0.55	0.56	0.54	0.54
V^{3+}	0.38	1.49	1.50	1.53	1.48	1.50	1.38	1.42	1.48	1.40	1.43	1.46
Fe	0.08	-	-	-	-	-	-	-	-	-	-	-
Total $(Al,V,Fe)^{3+}$	1.96	2.01	2.04	2.02	2.02	2.00	1.98	1.99	2.03	1.97	1.97	2.00
V^{4+}	1.84	2	2	2	2	2	2	2	2	2	2	2.00
Ti	0.16	-	-	-	-	-	-	-	-	-	-	-
Total $(V,Ti)^{4+}$	2	2	2	2	2	2	2	2	2	2	2	2.00
Si	2	2.02	1.98	1.98	1.98	1.98	2.01	2.00	1.98	2.00	2.01	2.00
$V^{3+}/(V+Fe+Al)^{3+}$	0.19	0.74	0.74	0.76	0.73	0.75	0.70	0.71	0.73	0.71	0.73	0.73
Y/(REE+Y+Sc)	0.72	0.62	0.63	0.63	0.63	0.63	0.63	0.63	0.64	0.63	0.63	0.63

*The VO_2 and V_2O_3 contents were calculated based on the basis that V^{4+} is ideally 2 apfu.

**The H_2O content was calculated on the basis of stoichiometry (i.e., OH = 4 apfu).

<mdl means below the minimum detection limit. Data for jingwenite-(Y) (Jw-Y) from Liu et al. (2023).

Table 3. Information on crystal and structural refinement for wenlanzhangite-(Y).

Crystal data	
Ideal chemical formula	$Y_2V^{3+}{}_2V^{4+}{}_2(SiO_4)_2O_4(OH)_4$
Crystal size/mm	0.02 × 0.01 × 0.005
Crystal system	Triclinic
Space group	*P*-1 (#2)
Unit cell dimensions	*a* = 5.9632(7) Å *b* = 9.5990(10) Å *c* = 9.9170(9) Å *α* = 90.033(8)° *β* = 98.595(9)° *γ* = 90.003(9)°
Volume	561.28(10)Å^3
Z	2
Density (calculated)	4.54 g/cm^3
Data collection and refinement	
Instrument	Rigaku-Oxford diffraction XtaLAB PRO-007HF
Radiation, wavelength, temperature	Mo*K*α, 0.71073, 293(2) K
2θ range (°)	5.938 to 58.414
μ /mm^{-1}	14.448
F(000)	676
Total reflections	6438
Unique ref (all)	2583
Unique ref [$I \geq 2\sigma(I)$]	1998
R_{int}	0.0494
R_σ	0.0587
Range of *h*, *k*, *l*	$-8 \leq h \leq 8$; $-12 \leq k \leq 13$; $-12 \leq l \leq 13$
R_1, wR_2 [$I \geq 2\sigma(I)$]	R_1 = 0.0736, wR_2 = 0.1813
R_1, wR_2 [all data]	R_1 = 0.0944, wR_2 = 0.1949
Goodness-of-fit	1.090
No. of parameters, restraints	244, 19
Max./min. residual peak (e Å^{-3})	5.51/-2.90

Table 4. Site, Wyckoff position (*W.p.*), site occupancy (s.o.), fractional atomic coordinates and equivalent isotropic (and anisotropic) displacement parameters (Å^2) for wenlanzhangite-(Y).

Sites	*W.p.*	*x*	*y*	*z*	s.o.	U_{eq}
Y1	2*i*	0.56987(12)	0.49227(8)	0.31186(8)	0.70(2)Y+0.312(15)Dy	0.0127(3)
Y2	2*i*	-0.16344(13)	-0.00777(9)	0.31188(8)	0.74(2)Y+0.273(15)Dy	0.0135(3)
Dy3	2*i*	0.092(4)	0.492(2)	0.312(2)	0.021(3)	0.009(9)
Dy4	2*i*	0.678(4)	0.004(3)	0.690(3)	0.026(4)	0.028(9)
V1	2*i*	0.3986(3)	0.2206(2)	0.4849(2)	0.84(3)V+0.16(3)Al	0.0145(7)
V2	2*i*	0.9063(3)	0.2786(2)	0.5143(2)	0.82(3)V+0.18(3)Al	0.0145(8)
V3	2*i*	-0.2457(3)	0.4960(2)	-0.0029(2)	0.83(3)V+0.17(3)Al	0.0154(8)
V4	1*a*	1	0	1	0.93(4)V+0.07(4)Al	0.0110(9)
V5	1*d*	0.5	0	1	0.52(3)V+0.48(4)Al	0.0134(12)
Si1	2*i*	0.0503(5)	0.2859(3)	0.2177(3)	1	0.0144(8)
Si2	2*i*	0.6914(5)	0.2111(3)	0.7817(3)	1	0.0135(8)
O1	2*i*	0.4475(12)	0.1776(8)	0.6845(8)	1	0.0136(16)
O2	2*i*	-0.1465(11)	0.3203(8)	0.3151(8)	1	0.0153(17)
O3	2*i*	0.0317(13)	0.1216(8)	0.1701(8)	1	0.0145(16)
O4	2*i*	0.6976(13)	0.3761(8)	0.8303(9)	1	0.0194(18)
O5	2*i*	0.8992(12)	0.1828(8)	0.6919(8)	1	0.0139(16)
O6	2*i*	0.3007(11)	0.3136(8)	0.3097(8)	1	0.0157(17)
O7	2*i*	0.7286(12)	0.1098(9)	0.9162(8)	1	0.0163(17)
O8	2*i*	0.0206(12)	0.3882(8)	0.0814(8)	1	0.0155(17)
O9	2*i*	0.1051(12)	0.1231(9)	0.4738(9)	1	0.0191(18)
O10	2*i*	1.1332(14)	0.3827(9)	0.5582(9)	1	0.0220(19)
O11	2*i*	0.6172(13)	0.3729(8)	0.5260(8)	1	0.0160(17)
O12	2*i*	0.6048(14)	0.1151(9)	0.4396(9)	1	0.0217(18)
O13	2*i*	-0.4808(12)	0.3955(8)	0.0855(8)	1	0.0157(17)
O14	2*i*	0.2327(12)	0.1065(9)	0.9144(8)	1	0.0152(17)
O15	2*i*	0.5490(13)	0.1142(9)	1.1570(9)	1	0.0212(19)
O16	2*i*	-0.2182(12)	0.6092(9)	0.1566(9)	1	0.0185(18)

Sites	U^{11}	U^{22}	U^{33}	U^{23}	U^{13}	U^{12}
Y1	0.0129(5)	0.0203(5)	0.0056(4)	-0.0012(3)	0.0037(3)	-0.0011(3)
Y2	0.0139(5)	0.0216(6)	0.0067(5)	-0.0009(3)	0.0069(3)	-0.0014(3)
V1	0.0137(11)	0.0251(14)	0.0053(10)	0.0018(8)	0.0033(7)	-0.0057(8)
V2	0.0142(11)	0.0251(14)	0.0059(11)	0.0031(8)	0.0069(7)	0.0062(8)
V3	0.0118(12)	0.0276(16)	0.0077(13)	-0.0001(10)	0.0049(8)	-0.0020(8)
V4	0.0111(14)	0.0174(17)	0.0056(14)	0.0001(10)	0.0046(9)	0.0001(10)
V5	0.0121(18)	0.019(2)	0.0106(19)	0.0021(14)	0.0061(12)	0.0005(12)
Si1	0.0125(15)	0.0213(17)	0.0106(15)	-0.0026(12)	0.0055(11)	-0.0016(12)
Si2	0.0139(15)	0.0213(17)	0.0063(14)	0.0004(12)	0.0050(11)	0.0000(12)
O1	0.015(3)	0.021(4)	0.006(3)	-0.002(3)	0.007(3)	-0.004(3)
O2	0.007(3)	0.028(5)	0.011(4)	0.004(3)	0.006(3)	0.001(3)
O3	0.026(4)	0.014(4)	0.005(4)	0.002(3)	0.006(3)	-0.001(3)

O4	0.026(4)	0.017(4)	0.015(4)	0.003(3)	0.004(3)	0.005(3)
O5	0.020(4)	0.018(4)	0.006(3)	-0.003(3)	0.007(3)	-0.001(3)
O6	0.009(3)	0.029(5)	0.009(4)	0.000(3)	0.004(3)	0.002(3)
O7	0.017(4)	0.027(5)	0.006(4)	-0.001(3)	0.004(3)	0.000(3)
O8	0.012(3)	0.021(4)	0.015(4)	-0.002(3)	0.006(3)	-0.001(3)
O9	0.019(4)	0.021(4)	0.018(4)	0.008(4)	0.005(3)	0.000(3)
O10	0.028(4)	0.026(5)	0.011(4)	0.003(3)	0.000(3)	-0.004(3)
O11	0.025(4)	0.017(4)	0.007(4)	0.001(3)	0.006(3)	0.001(3)
O12	0.027(4)	0.027(5)	0.013(4)	-0.001(3)	0.011(3)	0.002(3)
O13	0.013(3)	0.019(4)	0.016(4)	-0.003(3)	0.004(3)	-0.001(3)
O14	0.012(3)	0.028(5)	0.007(4)	-0.001(3)	0.006(3)	0.002(3)
O15	0.019(4)	0.034(5)	0.011(4)	-0.007(4)	0.003(3)	-0.005(3)
O16	0.017(4)	0.029(5)	0.012(4)	-0.008(3)	0.010(3)	0.001(3)

Table 5. Selected bond lengths (Å) for wenlanzhangite-(Y).

Y1|Dy1–O2[1]	2.360(7)	Y2|Dy2–O1[4]	2.355(7)	Dy3–O2	2.18(2)
Y1|Dy1–O4[2]	2.336(8)	Y2|Dy2–O3	2.316(7)	Dy3–O4[2]	2.39(2)
Y1|Dy1–O6	2.347(8)	Y2|Dy2–O5[5]	2.308(7)	Dy3–O6	2.12(2)
Y1|Dy1–O10[3]	2.357(8)	Y2|Dy2–O9[4]	2.376(8)	Dy3–O8	2.47(2)
Y1|Dy1–O11[2]	2.457(8)	Y2|Dy2–O9	2.439(8)	Dy3–O10[2]	2.33(2)
Y1|Dy1–O11	2.392(8)	Y2|Dy2–O12[6]	2.330(8)	Dy3–O10[6]	2.63(2)
Y1|Dy1–O13[1]	2.406(8)	Y2|Dy2–O14[4]	2.413(8)	Dy3–O11[2]	2.54(2)
Y1|Dy1–O16[1]	2.411(8)	Y2|Dy2–O15[7]	2.426(9)	Dy3–O16	2.49(2)
<Y1|Dy1–O>	**2.383**	**<Y2|Dy2–O>**	**2.370**	**<Dy3–O>**	**2.39**
Dy4–O1	2.15(2)	V1|Al1–O1	2.001(8)	V2|Al2–O2[1]	1.994(8)
Dy4–O3[5]	2.38(3)	V1|Al1–O6	1.963(8)	V2|Al2–O5	1.993(8)
Dy4–O5	2.16(3)	V1|Al1–O9	1.973(8)	V2|Al2–O9[1]	1.984(8)
Dy4–O7	2.44(3)	V1|Al1–O10[6]	2.407(9)	V2|Al2–O10	1.686(9)
Dy4–O9[5]	2.53(3)	V1|Al1–O11	1.961(8)	V2|Al2–O11	1.966(8)
Dy4–O12	2.67(3)	V1|Al1–O12	1.704(9)	V2|Al2–O12	2.418(9)
Dy4–O12[5]	2.27(3)	**<V1|Al1–O>**	**2.002**	**<V2|Al2–O>**	**2.007**
Dy4–O15[8]	2.46(3)				
<Dy4–O>	**2.38**				
V3|Al3–O4[7]	2.001(9)	V4|Al4–O3[5]	2.036(8)	V5|Al5–O7[8]	2.000(8)
V3|Al3–O8	1.974(8)	V4|Al4–O3[11]	2.036(8)	V5|Al5–O7	2.000(8)
V3|Al3–O8[9]	1.989(8)	V4|Al4–O7	2.005(7)	V5|Al5–O14[8]	1.976(7)
V3|Al3–O13	2.009(8)	V4|Al4–O7[12]	2.005(7)	V5|Al5–O14	1.976(7)
V3|Al3–O13[10]	2.004(7)	V4|Al4–O14[8]	2.011(8)	V5|Al5–O15	1.890(8)
V3|Al3–O16	1.906(8)	V4|Al4–O14[1]	2.011(8)	V5|Al5–O15[8]	1.890(8)
<V3|Al3–O>	**1.981**	**<V4|Al4–O>**	**2.017**	**<V5|Al5–O>**	**1.955**
Si1–O2	1.661(8)	Si2–O1	1.652(8)		
Si1–O3	1.645(8)	Si2–O4	1.654(9)		
Si1–O6	1.651(8)	Si2–O5	1.653(8)		
Si1–O8	1.659(9)	Si2–O7	1.639(8)		
<Si1–O>	**1.654**	**<Si2–O>**	**1.650**		

Symmetry codes: (i)1+X,+Y,+Z; (ii) 1-X,1-Y,1-Z; (iii) 2-X,1-Y,1-Z; (iv) -X,-Y,1-Z; (v) 1-X,-Y,1-Z; (vi)-1+X,+Y,+Z; (vii)-1+X,+Y,-1+Z; (viii) 1-X,-Y,2-Z; (ix) -X,1-Y,-Z; (x) -1-X,1-Y,-Z; (xi) 1+X,+Y,1+Z; (xii) 2-X,-Y,2-Z

Table 6. Comparison between wenlanzhangite-(Y) and jingwenite-(Y)

	Jingwenite-(Y)	Wenlanzhangite-(Y)
Ideal Formula	$Y_2Al_2V^{4+}{}_2(SiO_4)O_4(OH)_4$	$Y_2V^{3+}{}_2V^{4+}{}_2(SiO_4)_2O_4(OH)_4$
Z	4	2
Crystal System	Monoclinic	Triclinic
Space Group	*I*2/*a* (#15)	*P*-1 (#2)
$V^{3+}/(V^{3+}+Al+Fe^{3+})$	0.19	0.58-0.72 (mean = 0.67)
Unit-cell parameters	*a* = 9.4821(2)Å *b* = 5.8781(1) Å *c* = 19.3987(4) Å *β*= 90.165(2)° *V*= 1081.21(4) Å^3	*a* = 5.9632(7)Å *b* = 9.599(1) Å *c* = 9.9170(9) Å *α* = 90.033(8)° *β* = 98.595(9)° *γ* = 90.003(9)° *V*= 561.28(10) Å^3
Reference	Liu *et al*. (2023)	This study